Modeling the size of co-seismic landslides via data-driven models: the Kaikōura's example

Mateo Moreno[1,2*], Stefan Steger[1], Hakan Tanyas[2], Luigi Lombardo[2]

Abstract

The last three decades have witnessed a substantial methodical development of data-driven models for landslide prediction. However, this improvement has been dedicated almost exclusively to models designed to recognize locations where landslides may likely occur in the future. This notion is referred to as landslide susceptibility. However, the susceptibility is just one, albeit fundamental, information required to assess landslide hazard and to mitigate the threat that landslides may pose to human lives and infrastructure. Another complementary and equally important information is how large landslides may evolve into, once they initiate in a given slope. Only three scientific contributions have currently addressed the geographic estimation of how large co-seismic landslides may be. In the first one, the authors tested a model solely at the global scale, whereas the remaining two involved specific regional scale settings. The low number of previous research on the topic as well as specificities related to the associated study areas do not yet allow to fully support a standardized use of such models. In turn, this has repercussions on the operational feasibility and adoption potential of data-driven models capable of estimating landslide size in site-specific conditions. This manuscript addresses this gap in the literature, by further exploring the use of a Generalized Additive Model whose target variable is the topographically-corrected landslide extent aggregated at the slope unit level. In our case, the underlying assumption is that the variability of the landslide sizes across the geographic space behaves according to a Log-Normal probability distribution. We test this framework by going beyond the conventional non-spatial validation scheme in order to take a particularly critical look at the estimated model performance. The study focuses on co-seismic landslides mapped as a result of the ground motion generated by the Kaikōura earthquake (11:02 UTC, on November 13^{th} 2016). The experiment led to further insights into the applicability of such approaches and produced more than satisfying performance scores, which we stress here in the prospect of stimulating further research towards spatially-explicit landslide size prediction.

In line with the same idea, we share data and codes in a github repository (link here) to promote repeatability and reproducibility of this research.

Keywords: Kaikōura Earthquake; Landslide area prediction; Landslide hazard; Slope unit partition

[1]Eurac Research, Institute for Earth Observation, Bolzano-Bozen, 39100, Italy

[2]University of Twente, Faculty of Geo-Information Science and Earth Observation (ITC), Enschede, AE 7500, Netherlands

1 Introduction

The estimation of where landslides may occur in the future has dominated the geomorphological literature pertaining to data-driven applications since its first conceptualization in the early 1970's (Reichenbach et al., 2018). Almost no other data-driven modeling framework with a spatially-explicit connotation has been developed for the subsequent five decades other than the susceptibility (Van Westen et al., 2003; Fell et al., 2008). This concept boils down to the estimation of the probability of a landslide occurring in a given mapping unit under the influence of topography and other thematic landscape characteristics (Brenning, 2005; Van Westen et al., 2008). An extension to this framework is present in the literature, although less prominent than the susceptibility, and it features the spatio-temporal characteristics of the landslide trigger, leading to the estimation of the hazard concept (Guzzetti et al., 1999). This extension has led to the development of important forecasting tools such as near-real-time models (Lombardo and Tanyas, 2020; Nowicki Jessee et al., 2018) and early-warning-systems (Intrieri et al., 2012; Kirschbaum and Stanley, 2018). In both cases though, the model behind the respective results still targets landslide occurrence data in the form of presences or absences across a given landscape (Frattini et al., 2010).

In this context, as the technology advanced, the information on unstable slopes also changed, being acquired and processed in multiple ways. For instance, at the origin of the susceptibility concept, geomorphologists were observing the landscape and labeling slopes to be likely stable or unstable on the basis of their personal experience (Brabb et al., 1972). Right after that, the birth of GIS facilitated the development of numerical tools, which started from simple analytical approaches such as bivariate statistics (e.g., Van Westen et al., 1997; Ayalew et al., 2005; Nandi and Shakoor, 2010) and evolved into more complex modelling schemes where multiple variable simultaneously contribute to estimate the susceptibility (e.g., Atkinson and Massari, 1998; Lee et al., 2008; Steger et al., 2016). The latter frameworks belong to two very different and complementary approaches that have taken root in the landslide community. One corresponds to the use of statistical models where model interpretability is often favored at the expense of reduced model flexibility and lower performance scores (i.e., analytical task). And the other one, corresponding to the field of machine learning, where performance maximization is sought instead, at the expense of interpretability (i.e., prediction task). Two common examples respectively correspond to statistical models such as Generalized Linear Models (e.g., Castro Camilo et al., 2017) and to machine learning models such as decision trees (e.g., Yeon et al., 2010) or neural networks (e.g., Wang et al., 2021). In between these two lies the Generalized Additive Model, also referred to as an interpretable machine learning technique (Goetz et al., 2011; Steger et al., 2021). They still ensure a high degree of interpretability tipical of statistical architectures, but their structure allows for incorporating nonlinear effects, which in turn leads to flexible models with high performance (Steger et al., 2017; Lin et al., 2021). Nevertheless, because their target variable is a binary realization of landslide occurrences, these spatially-explicit models lack the ability to return the information on how large a landslide may be (Lombardo et al., 2021), or on how many coalescing landslides may initiate in a particular region (Lombardo et al., 2019). Only three articles currently exist where a data-driven and spatially-explicit model is capable of estimating landslide sizes. The first one was recently published by Lombardo et al. (2021), and the authors proposed it to estimate either the maximum or the sum of landslide planimetric areas within slope units (Carrara, 1988). However, despite the novel perspective provided by the authors, a substantial weakness characterized their work. In fact, the model they propose has a global connotation. This implies that knowing its validity in a worldwide context is not sufficient because this scale is far from being applicable to local territorial management practices. In other words, the applicability of the model proposed by Lombardo et al. (2021) still needs to be validated for site-specific conditions. Moreover, it needs to undergo several tests both in case of seismic- and rainfall-induced landslides. To this purpose, the two remaining contributions have tried to replicate a similar experimental setting at regional scales, one focusing on co-seismic landslides (Aguilera et al., 2022) and one on rainfall-triggered (Bryce et al., 2022) ones. However, the academic process that the modeling of landslide susceptibility has undergone before becoming a standard across the geoscientific community has required thousands of contributions. The three previous works focusing on the prediction of landslide planimetric extents are definitely not sufficient to transfer and implement this knowledge at the core of international policies. This is why in this work, we sought to produce a new experiment that follows the main workflow direction of the three articles mentioned above, but simultaneously introduces not yet tested methodical innovations, such as the topographic correction of the landslide size target variable or the critical validation of model performances using a spatially-explicit model validation technique. Specifically, we selected the Kaikōura earthquake (7.8 M_w, 13-11-2016), for which a co-seismic landslide inventory has been recently made publicly available (Tanyas et al., 2022). We partitioned the area affected by landslides into slope units (Alvioli et al., 2016), extracted the sum of all landslide extents falling within each mapping unit and calculated the topographically-corrected surface area. As for the model, we adopted a Generalized Additive Model structure under the assumption that the aggregated landslide area per slope unit behaves according to a Log-Gaussian likelihood (cf. Lombardo et al., 2021).

2 Study area overview

2.1 Study area and co-seismic landslides

The Kaikōura earthquake struck the South Island of New Zealand on the 14^{th} of November 2016 at 11:02 UTC. This was not only the largest magnitude crustal earthquake in New Zealand that occurred in more than 150 years, but also a unique event showing an extremely complex rupturing mechanism (Hamling et al., 2017; Ulrich et al., 2019). The earthquake cascaded across a series of fault planes with dextral, sinistral, oblique and reverse rupturing mechanisms (Diederichs et al., 2019). Significant co-seismic surface deformations were reported in a large landscape extending up to 100 km far from the epicenter (Cesca et al., 2017).

Specifically, the reported uplift amount reached up to 8 meters in some locations (Hamling et al., 2017). As a result, the earthquake had severe repercussions on both infrastructure and the environment itself (Kaiser et al., 2017).

Considering the steep mountainous terrain affected by this considerable ground shaking, unsurprisingly, the earthquake also resulted in a large number of landslides (Massey et al., 2018, 2020; Tanyas et al., 2022). Massey et al. (2020) reported more than 29,000 landslides triggered by the earthquake, whereas Tanyas et al. (2022) mapped 14,233 landslides over a total area of approximately 14,000 km^2. Considering the documented earthquake-induced landslide events (Fan et al., 2018; Tanyaş et al., 2017; Tanyaş et al., 2022), the Kaikōura event is one of the largest ever recorded in the literature.

This study examines the area affected by the 2016 Kaikōura earthquake and, specifically, the landslide inventory mapped by Tanyas et al. (2022). The authors delineated landslides' sources and deposit areas as single polygons. The inventory consists of various landslide types and materials, including disrupted rock, debris, soil falls and slides. However, landslide types are not indicated in the original data source, and thus, our analyses are not sensitive to any specific type of landslides.

2.2 Slope Units

The use of a Slope Unit (SU) delineation in the framework of landslide predictive models dates back to Carrara (1988). The spatial extent of this mapping unit is usually coarser than the more common grid cells. The latter are regular polygonal objects that offer a simple spatial partition of any landscape, mainly by matching the gridded resolution of the Digital Elevation Model available for the given study area. To express the spatial variability of continuous phenomena, such as temperature fields, they are perfectly suitable. However, landslides are discrete processes. As a result, the geoscientific community has long debated whether grid cells are actually suitable for modeling slope failures. Conversely, SUs are more suitable from a geomorphological perspective, although they require additional pre-processing steps such as the aggregation of fine-scaled landscape characteristics. This is the reason why SUs have gained more attention in recent years with more and more articles using this specific partition. Moreover, several automated tools have been proposed and even freely shared within the geoscientific community (Alvioli and Baum, 2016; Huang et al., 2021). Their use so far has been almost uniquely dedicated to the estimation of landslide susceptibility. In this work, we select SUs to partition the area affected by the Kaikōura earthquake to predict the cumulated extent of landslides per mapping unit. To promote repeatability of the analyses, below we report the parameterization of *r.slopeunits*, the software we used. As for their interpretation, we refer to Alvioli et al. (2016).

- Circular variance = 0.4
- Flow accumulation threshold = 1,000,000
- Minimum Slope Unit area = 80,000
- Cleansize = 50,000

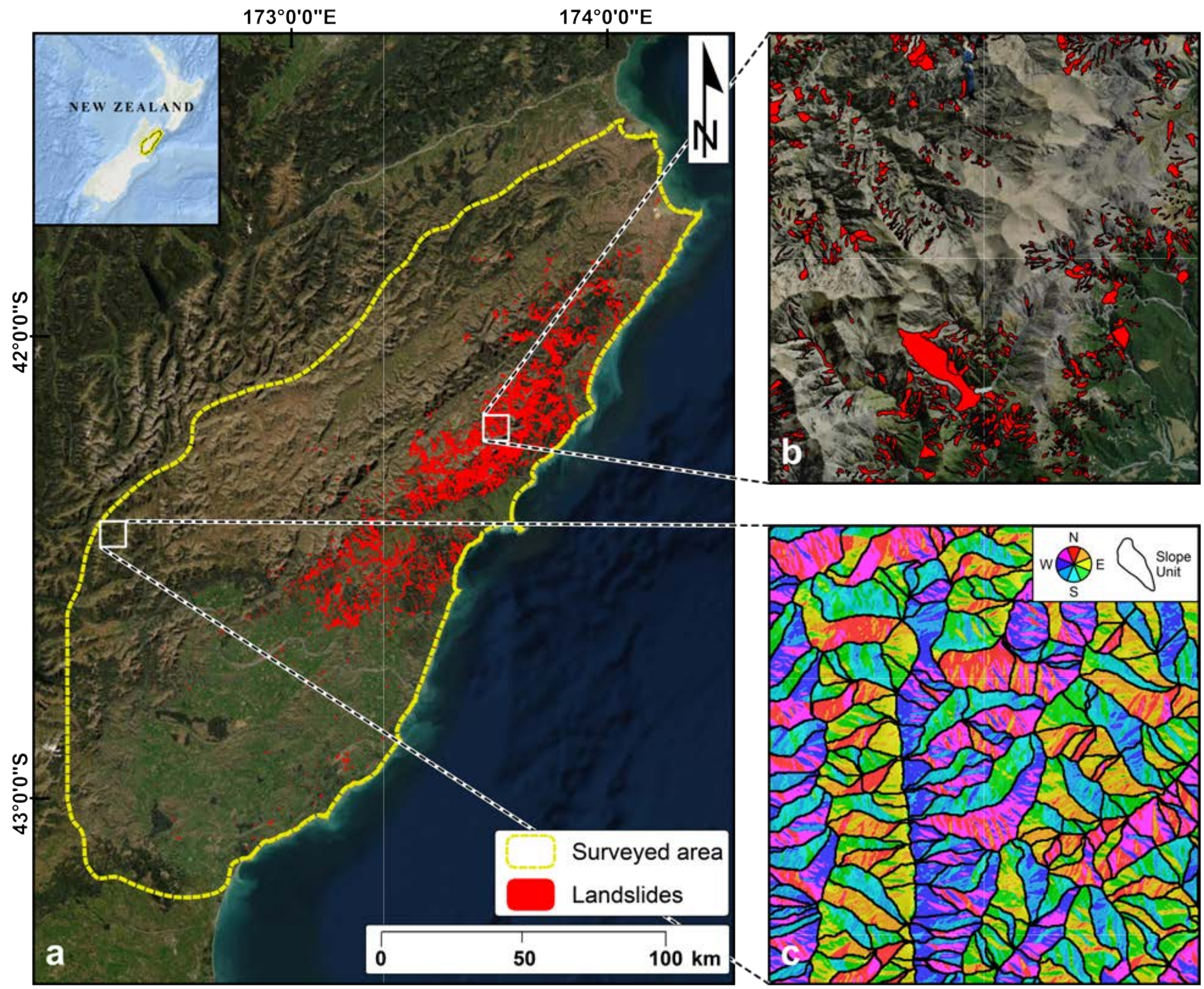

Figure 1: Geographic summary of the co-seismic landslides triggered in response to the Kaikōura earthquake (panels a and b). Panel c shows an example of the slope unit delineation superimposed onto the aspect map.

The resulting SUs offered a medium resolution of the landscape exposed to the Kaikōura landscapes with 26,839 total SUs, whose size distribution has a mean of 500,000 m^2 and a standard deviation of 430,000 m^2.

2.3 Covariates: landscape characteristics and ground motion data

This section illustrates the covariates we adopted to explain the variability of the co-seismic landslide area distribution in Kaikōura. Although there is an extensive literature examining factors governing the probability of spatial landslide occurrence, factors controlling the size of landslides in a spatial context is a relatively new concept (e.g., Lombardo et al., 2021). In this regard, we tested several variables representing morphometric, anthropogenic and seismic factors as well material properties (see Table 1). We tested some basic DEM derivatives namely, slope steepness (Slope), northness (NN), eastness (EN), local relief (Relief), profile curvature (PRC) and planar curvature (PLC) to assess the role of morphometric variables on landslide size. Capturing the role of anthropogenic factors is often challenging (e.g., Tanyaş et al., 2022) but the area affected by the earthquake is a remote territory, and the road cuts are the main features representing human influence on landsliding. Therefore, we calculated the Euclidean distance to the road network (e.g., Lepore et al., 2012) to capture the possible influence of anthropogenic factors. Specifically, we accessed the road network map of the study area via Land Information Portal (https://data.linz.govt.nz) of New Zealand. As for the co-seismic ground shaking, we used Peak Ground Acceleration (PGA) map of the Kaikōura earthquake provided by the U.S. Geological Survey (USGS) ShakeMap system (Worden and Wald, 2016). PGA is a seismic proxy, and specifically, the deterministic estimate of PGA provided by the USGS ShakeMap system is widely used in susceptibility analyses of co-seismic landslides (e.g., Nowicki et al., 2014; Godt et al., 2008). Also, we used the soil thickness map of the study area, which is a proxy for the shear strength of hillslope materials. We accessed the soil thickness map (Lilburne et al., 2012) of the study area via The Land Resource Information System Portal of New Zealand (https://lris.scinfo.org.nz). Different from the all the other covariates, we examined the soil thickness map as a categorical covariate because it includes four categories where soil depth is described as deep (D, >90 cm), moderately deep (MD, 40-90 cm), shallow (S, 20-40 cm) and very shallow (VS, <20 cm) as well as a category indicating no soil cover (NS).

2.4 Data aggregation at the Slope Unit level

We used slope units to aggregate both the target variable, this being the topographically-corrected landslide area, and the covariates described in the previous Section.

The landslide extent calculation was based on the aggregation of the landslide area by summing up all landslide areas within each SU. Before this aggregation step though, we applied a correction procedure to reduce the underestimation of landslide size on steeper terrain due to the underlying conventional planar projection. For this purpose, a trigono-

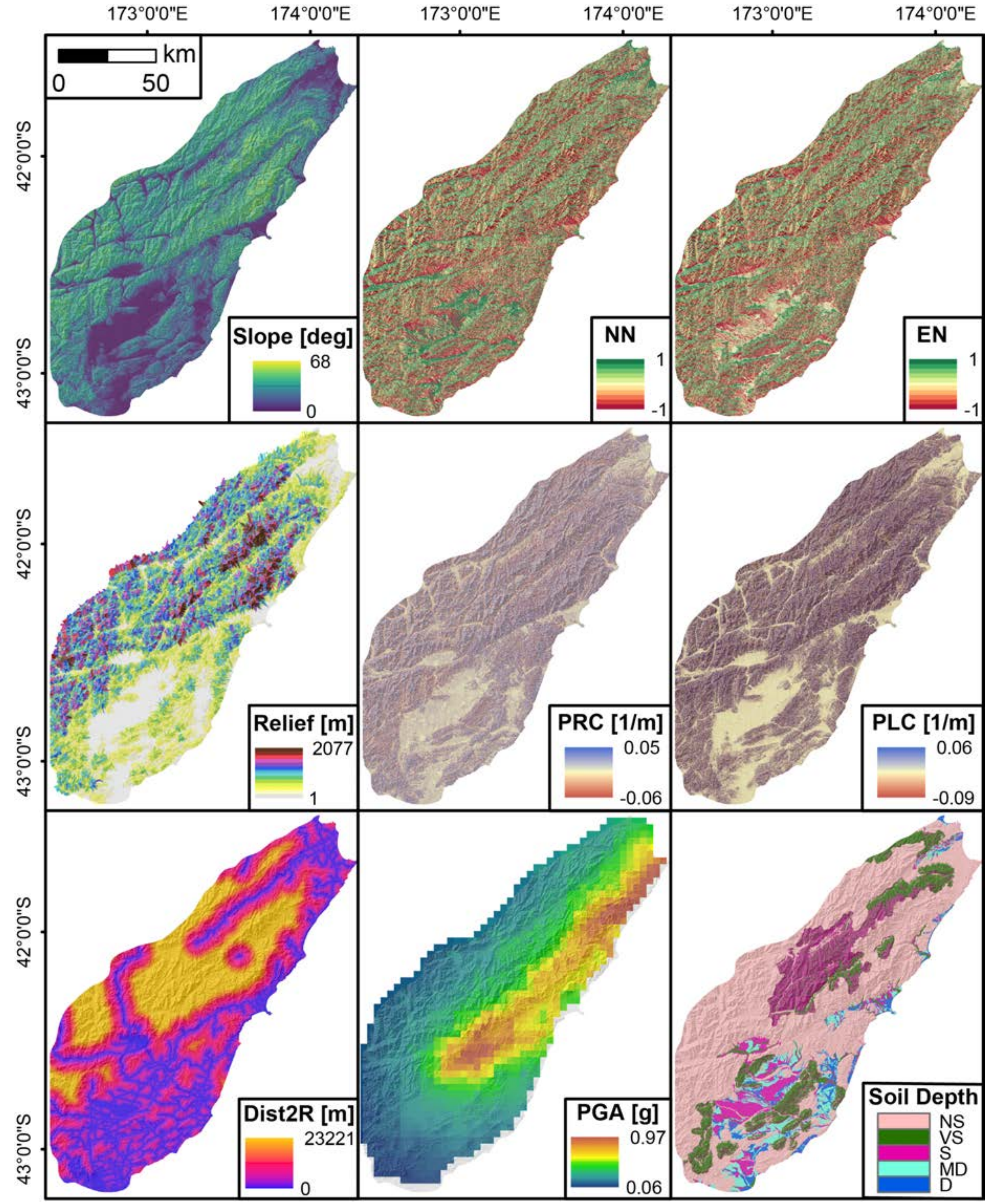

Figure 2: Example of the covariate set used for the analyses. The soil depth map includes five classes namely, NS for No Soil, VS for Very Shallow, S for Shallow, MD for Moderately Deep and D for Deep. Notably, the Dist2R map is shown as is only for graphical purposes. We actually constrained the information conveyed by Dist2R (to the model we will describe in Section 3) only up to a 500m buffer around the road network. After this distance we impose the covariate to cease to be informative.

Table 1: Covariates' summary table. Each covariate listed here was later used during the analyses in a dual form. Specifically, we represented each covariate in this table through the mean and standard deviation values computed per SU. We do not list both terms in the table, but they will be denoted in the remainder of the manuscript via the suffix _mean and _stdev added to the acronyms reported in table.

Variable	Acronym	Reference
Slope steepness	Slope	(Zevenbergen and Thorne, 1987)
Northness	NN	e.g., (Loche et al., 2022)
Eastness	EN	e.g., (Loche et al., 2022)
Local relief	Relief	(Jasiewicz and Stepinski, 2013)
Profile curvature	PRC	(Heerdegen and Beran, 1982)
Planar curvature	PLC	(Heerdegen and Beran, 1982)
Euclidean distance to road	Dist2R	e.g.,(Lepore et al., 2012)
Peak ground acceleration	g (m/s^2)	(Worden and Wald, 2016)
Soil depth	Soil Depth	(Webb and Lilburne, 2011; Hewitt et al., 2010; Lepore et al., 2012)

metric function based on a slope angle map (grid cell resolution 12.5 x 12.5 m) was used to derive the "true" surface area of each landslide polygon in analogy to Steger et al. (2021).

Figure 3a shows the distribution of the topographically-adjusted landslide area after the aggregation step mentioned above (sum for each SUs). Being the distribution strongly heavy-tailed, we opted to gaussianize it by taking the logarithm of the cumulative landslide area per SU Figure 3b. In such a way, a Log-Gaussian model could be used to suitably explain the variability of these estimates (more details in Section 3.1).

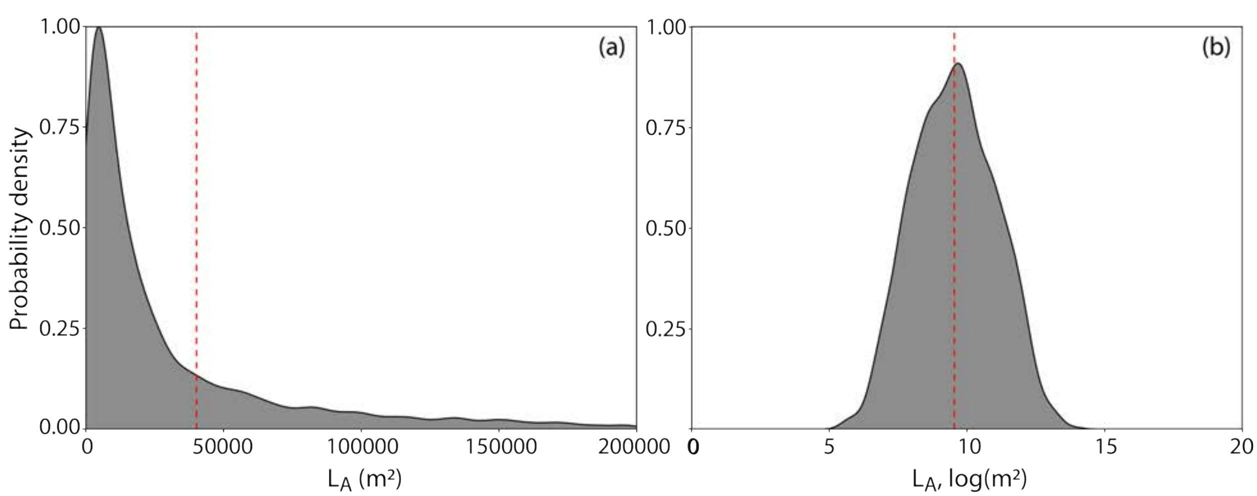

Figure 3: Distribution of the topographically-corrected landslide areas per SU. Panel (a) shows the sum of derived landslide areas per SU in a linear scale, whereas panel (b) highlights the same information in logarithmic scale.

As for the landscape characteristics, we computed the mean and standard deviation of the each continuous covariate per SU. Ultimately, whenever the landscape characteristics corresponded to categorical properties, such as underlying lithologies, land use or soil thickness classes, we only extracted the dominant type per SU.

3 Modeling strategy

Below we provide a brief description of the model we adopted, the cross-validation scheme we implemented and the metrics we used to assess how the estimated landslide areas matched the observed cases.

3.1 Generalized Additive Model

A Generalized Additive Model (GAM) can be seen as a flexible extension of a Generalized Linear Model (GLM). In analogy to GLMs, GAMs can handle a variety of error distributions but additionally allow one to account for nonlinear associations between the target variable and continuous predictors. This additional flexibility combined with high interpretability makes GAMs particularly useful for data-driven environmental studies. The presence of nonlinear relationships between landslide occurrence and environmental factors can be expected (e.g., landslides may less likely occur in flat and very steep terrain), while high interpretability of the modelling results is paramount for geomorphological interpretation and plausibility checks (Vorpahl et al., 2012; Steger et al., 2017; Brenning et al., 2015). GAMs with a binomial error distribution have been successfully applied to model landslide susceptibility (Petschko et al., 2014; Bordoni et al., 2020; Titti et al., 2021), while Poissonian GAMs were used to model spatial landslide counts (i.e. intensities; Lombardo et al., 2019, 2020). A Log-Gaussian distribution within a Bayesian GAM built the foundation to create the first data-driven model to predict landslide sizes per SUs, i.e., the maximum landslide size and the sum of landslide size (Lombardo et al., 2021). The Log-Gaussian GAM used within this study is based on the R-package "mgcv" (Wood and Augustin, 2002). This framework allowed us to model the topographically corrected log-size of co-seismic landslide areas at SU-level (hereafter L_A) as a function of a covariate set that describes landscape characteristics and spatial ground motion properties. The nonlinear relationships (i.e., selection of the amount of smoothness) were fitted using internal cross-validation (Hauenstein et al., 2018), while we restricted the maximum allowed flexibility of the underlying smoothing functions to a k-value of 4 (i.e. the maximum allowed degrees of freedom) to enhance model generalization and interpretability. The generated covariates are described in detail within Section 2.3, while their selection was based on a systematic procedure that included an iterative fitting and evaluation of different model realizations. In detail, we started with a full model and iteratively excluded covariates that did not meet the following two criteria: a covariate was only considered appropriate in case the underlying smoothing term was estimated to be significant at the five percent level (p-value ¡ 0.05); a covariate did not enhance the model's predictive performance.

Besides being able to handle nonlinear relationships, GAMs also allow one to visualize modelled associations. This model transparency is particularly useful to enable interpretation and to uncover implausible results (Zuur et al., 2009; Steger et al., 2021). In this sense, component smooth function (CSF) plots were used to visualize the estimated covariate-response relationship. These plots enabled an interpretation of modelled nonlinear effects on the aggregated landslide size per SU at a single covariate level while simultaneously accounting for the influence of the other covariates in the model (Zuur et al., 2009, 2010; Molnar, 2020).

3.2 Model performance

Below we provide a split summary of the cross-validation schemes we adopted and the metrics we used to assess how our model performed in explaining the spatial distribution of landslide areas. The last section explains how we then provided estimates of landslide areas for SU that did not experience slope failures during the Kaikōura earthquake.

3.2.1 Cross-validation routines

To test the performance of our model, we select two cross-validation approaches. The first corresponds to a purely random cross-validation scheme (RCV), where we repeatedly extracted a random subset of 90% SUs within the study area for training our model (i.e., training set) while the remaining data (i.e., test set) of each repetition was used to calculate the performance metric. We constrained the random selection to select the same SU only once. Thus, the union of the 10 replicates returns all the SU constituting the whole study area.

However, any spatial process usually embeds some degree of internal spatial dependence, which may not be fully explained by the covariate set one can choose. Conventional non-spatial random partitioning of training and test sets (e.g., RCV) may provide test statistics that do not capture the variability of model performance across sub-regions of a study site. Using RCV, overoptimistic performance scores are likely to be measured if spatial model predictions poorly match observational data within single sub-regions of an area. Spatially explicit validation schemes, such as spatial cross-validation (SCV), can be used to estimate the spatial transferability of model performance scores within a study site and uncover spatially incoherent model predictions (Steger et al., 2017). SCV results can inform potential users of a given model about worst-case prediction skills in space and about the spatial robustness of the general model setup. SCV is usually based on a repeated random splitting of training sets and test sets according to sub-areas of a study site. For this study, the underlying spatial partitioning approach is based on k-means clustering (see, Brenning, 2012; Schratz et al., 2019, for a more detailed explanation).

In this work, we opted to report the model performance estimated via a RCV where the prediction skill is aided by residual clustering effects, as well as via a SCV where the estimated performance scores are usually lower, thus providing insights into the minimum prediction skill one can expect for sub-regions of the study site. Figure 4 shows a few examples of the routines mentioned above. Specifically, the RCV and SCV have been repeated for 10-folds, including a component of 10 iterations to randomize the spatial cluster of slope units to be extracted.

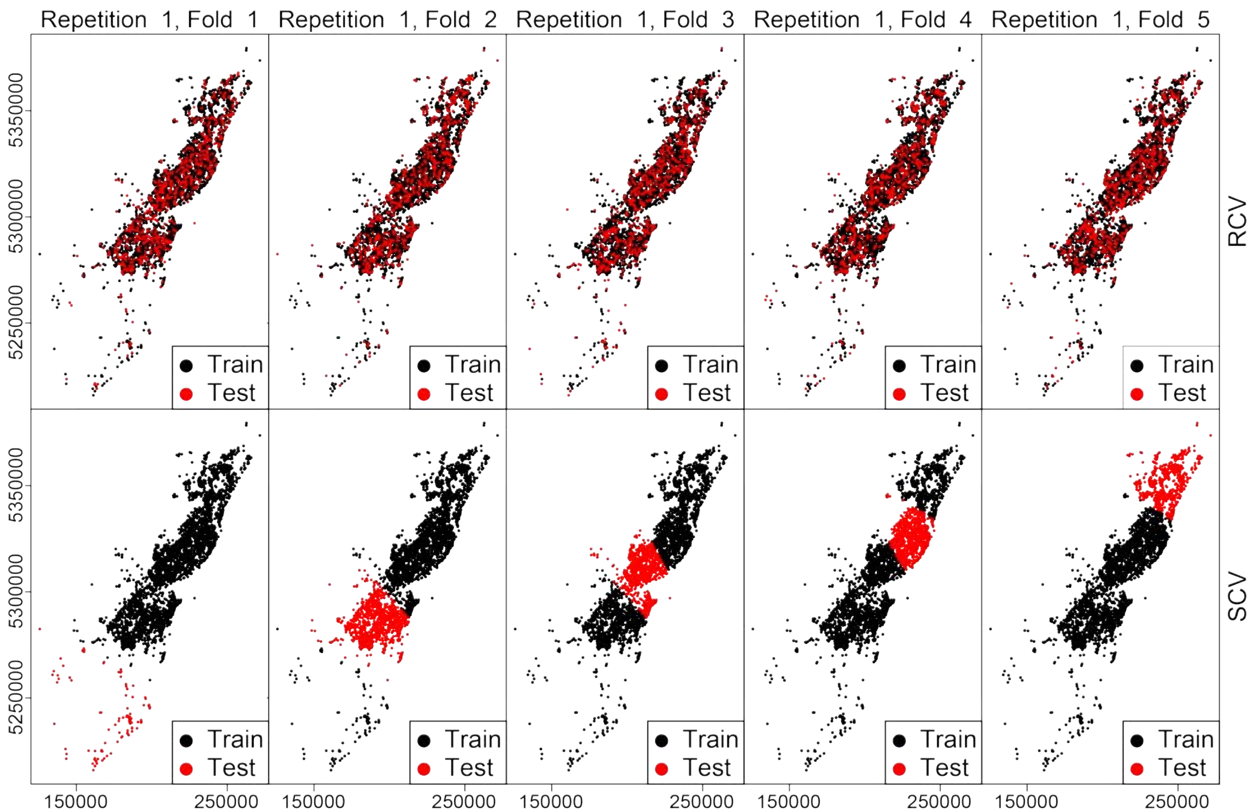

Figure 4: Geographical sketches of CV routines via five examples out of the XX CV folds we implemented in this work. The first row shows a RCV whereas the second row highlights the effect of a spatial constraint in the SU selection.

3.2.2 Performance metrics

To assess how suitable our modeling framework is to reflect the observed landslide area per SU, we selected a dual approach featuring visual and numerical performance summaries for both CV schemes described above. The visual summary corresponds to a simple graph where the observed landslide areas are plotted against the estimated ones. As for the numerical summaries, the metrics we opted for consist of the Pearson Correlation Coefficient (R-Pearson; Schober et al., 2018) and Mean Absolute Error (MAE; Mayer and Butler, 1993). To these, we also add the Root Mean Square Error (RMSE; Kenney and Keeping, 1962) for completeness, although the literature mentioned in several contributions that the MAE is a better measure of deviance (Willmott and Matsuura, 2005; Chai and Draxler, 2014).

3.3 Map-based landslide area prediction

In this section, we specify something of particular conceptual relevance. In fact, in traditional susceptibility models, one can and should use the presence-absence information across the whole study area (Petschko et al., 2014; Lombardo and Mai, 2018). However, the information on the landslide area is only associated with a subset of the SUs partitioning the Kaikōura landscape. Therefore, to produce maps of predicted landslide size for the whole study area, we adopted the following procedure. Initially, we extracted the positive landslide areas to train and test our Log-Gaussian GAM. Subsequently, we implemented a simulation step where we used the estimated regression coefficients to solve the predictive function in areas where the landslide area information was not available.

4 Results

Below we separately present the interpretation of the model components, performance and mapping results.

4.1 Model relationships

This section summarizes the estimated covariate effects responsible to explain the spatial distribution of landslide sizes per SU.

Figure 5 offers an overview of all the nonlinear effects we included in the model. Although we allowed the regression coefficient to vary nonlinearly across each covariate domain, the implemented internal smoothness selection procedure selected certain covariates to be best represented via linear functions. This is the case for *Slope_stdev*, *NN_mean*, *PRC_stdev* and *PGA_mean*. This implies that a unit increase in the covariate value would generate a proportional change – depending on the sign of the regression coefficient – onto the resulting landslide size. And, that the change would be the same irrespective of where that unit increase happens across the whole covariate spectrum. Moreover, eight covariates deviated from the linear behavior, out of which two were only mildly nonlinear *NN_stdev*, *Dist2R_stdev*), whereas the remaining six showed a much more evident nonlinear effect (*Slope_mean*, *EN_mean*, *Relief*, *PLC_mean*, *Dist2R_mean* and *PGA_stdev*).

Below we provide a brief overview of these covariate effects (from the most interesting linear to the nonlinear ones) by interpreting their marginal contribution (i.e., assuming all the other covariates' contributions to be fixed). For instance, we justify the positive increase of the estimated landslide size due to *Slope_stdev* because a rougher terrain can have larger quantities of hanging material susceptible to be mobilized due to the contextual water impoundment (Jiao et al., 2014). Similarly, the *PGA_mean* also positively contributes to the estimated landslide area, and its linear behavior can be naturally seen as the destabilizing effect of ground motion over the landscape (Tanyas and Lombardo, 2019). Furthermore, two covariates share a similar nonlinear contribution. These are *Relief* and *PLC_mean*, both with a pronounced sigmoidal behavior. The former can be interpreted with the positive contribution of the gravitational potential energy, where at increasing values, the failing mass will experience a further increase in kinetic energy as it moves downhill, thus producing larger landslides overall (Melosh, 1986; Yamada et al., 2018). As for *PLC_mean*, the planar curvature is known to control convergence effects of granular materials and overland waters flowing over the landscape (Ohlmacher, 2007).

Aside from covariates we allowed to behave nonlinearly while still carrying their ordinal structure, we also considered the nonlinear and categorical signal of soil thickness classes. As it stands out in Figure 6, the signal carried by the prevalent soil depth class per SU does not produce a clear "monotonic" pattern in the estimated regression coefficients per class (i.e., landslide size increases/decreases systematically with soil depth). This is likely due to two reasons. First, the raw soil depth map we accessed is directly expressed into classes, which implies a loss in the continuous information a soil depth should be expressed into. Clearly, a soil depth cannot be continuously measured over space because it would require excessive resources, and therefore, even the classes we used are the result of an interpolation routine, which may have smoothed the soil depth signal over space. Similarly, and we believe this to be a second and valid reason for the not straightforward to interpret effects emerging in Figure 6, we also applied a second level of hierarchical smoothing when we aggregated the soil depth signal over the SU by choosing the majority rule. In this sense, a given SU is assigned with the soil depth label of the class with the largest areal extent. However, the majority class may not be the one responsible for the failure.

4.2 Model performance

The visual agreement between observed and estimated landslide area among the three model routines we tested is summarized in Figure 7. There, one can see that the model fit produces the highest degree of agreement between the observed and estimated landslide areas. The second panel closely follows the trend shown for the fit, with the RCV predicted landslide areas almost aligning along the 45 degree dashed line. As for the SCV results, the deviations from a perfect match between observed and estimated landslide areas appears slightly more pronounced compared with the other two cases. However, this is to be expected because a SCV essentially takes away any residual dependence from a spatially distributed dataset, thus producing lower performance scores in a real-world data setting. In this sense, the match shown for the SCV can still be considered suitable and a valuable source of information for hazard assessment.

Figure 8 complements the previous plot by informing on the correlation between observed and estimated landslide areas, together with the error between the two. Several authors have proposed a classification of the R-Pearson, and most of the literature on the topic would indicate values of around 0.6 to reflect a moderate (Mm, 2012) to strong (Corder and Foreman, 2011) correlation between observed and estimated landslide extents. Analogous considerations arise by examining the MAE and RMSE, with acceptable errors in both the

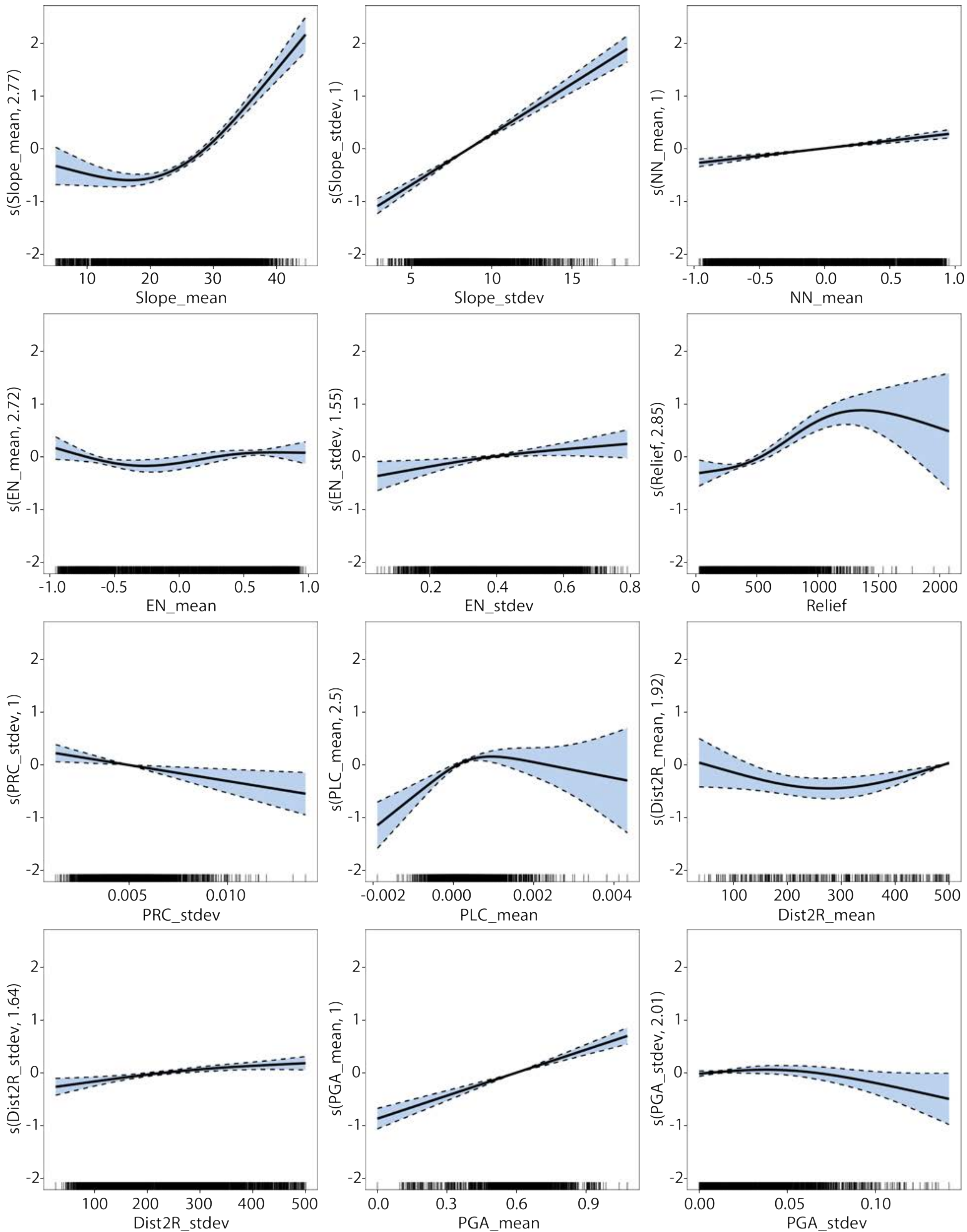

Figure 5: Summary of ordinal nonlinear effects on the aggregated landslide size per SU.

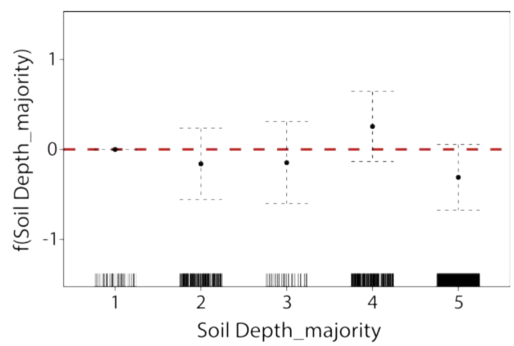

Figure 6: Summary of categorical nonlinear effect of soil depth classes on the aggregated landslide size per SU.

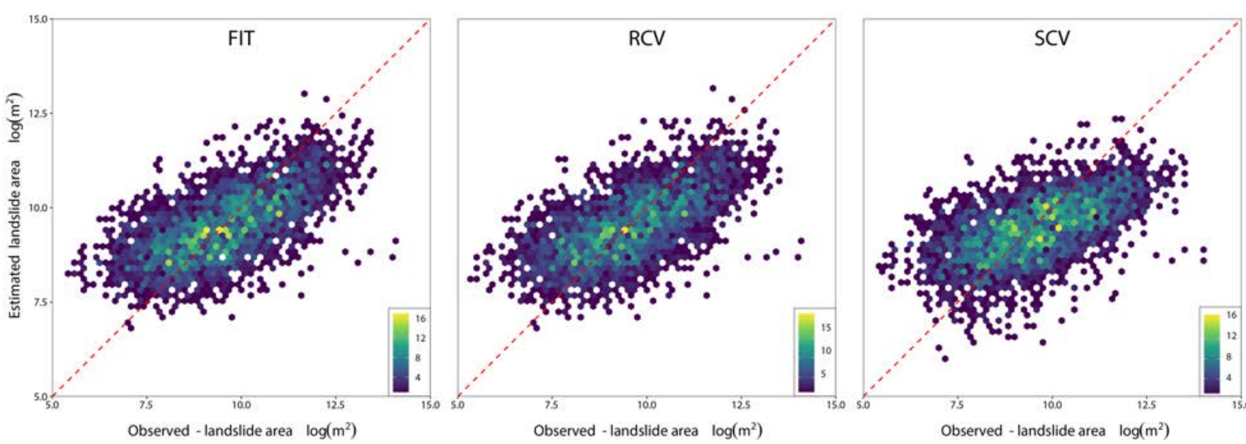

Figure 7: Summary of the agreement between observed landslide area per SU and the corresponding values estimated through a fit where all the information was used and two cross-validations (RCV and SCV) where part of the information was iteratively extracted solely for testing purposes.

cross-validation schemes. Notably, the performance metrics reported in Figure 8 confirm that the SCV returned a slightly poorer agreement compared to a purely random cross-validation scheme.

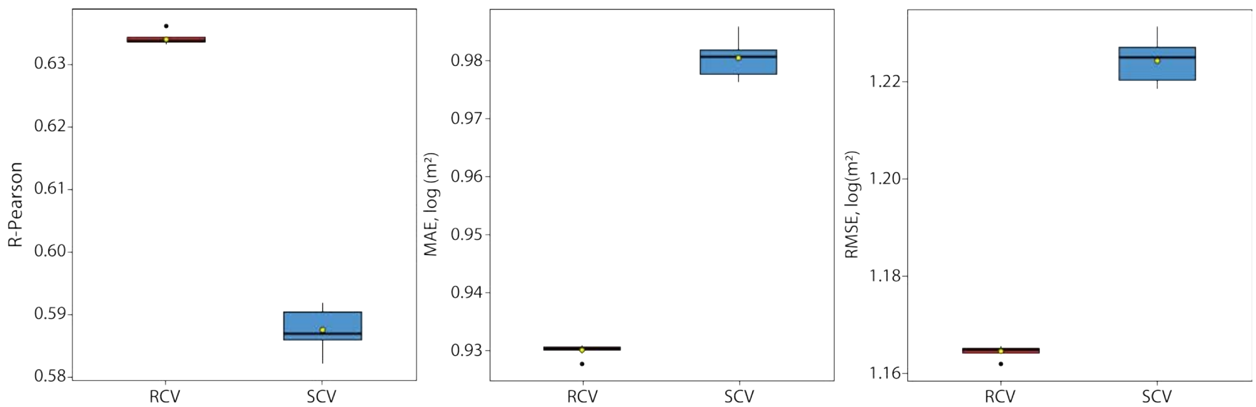

Figure 8: Pearson correlation coefficient, mean absolute error and root mean square error estimated for the purely random cross-validation and the spatial random cross-validation, respectively.

4.3 Landslide area predictive maps

Fitting a statistical model allows one to retrieve the set of regression coefficients through which one can estimate the expected values of the given target variable. At the same time though, one can use the same set of regression coefficients to solve the predictive function for locations where the target variable is not known. The latter concept boils down to what one would refer to as a statistical simulation (e.g., Lombardo and Tanyas, 2021; Luo et al., 2021) or model transferability (e.g., Petschko et al., 2014; Steger et al., 2017). Figure 9 summarizes the estimates produced through the RCV and SCV at SU for which we have actual L_A observations, as well as SU where we have not. The first row highlights the agreement in spatial patterns among the observed and predicted L_A values, with a coherent pattern shown among the three images, albeit the prediction routines show some degree of smoothing as they transition from RCV to SCV. The strength of our modeling framework is particularly highlighted in the second row of Figure 9 where we transferred the predictive equations to the remained of the Kaikōura's landscape.

5 Discussion

The capacity of data-driven models to go beyond traditional susceptibility models is still at an infancy stage. This experiment has shown that a Log-Gaussian GAM is able to reproduce the pattern and value range of landslide areas aggregated at the slope unit level. Out of the whole procedure, certain elements already support the replication of similar analyses while

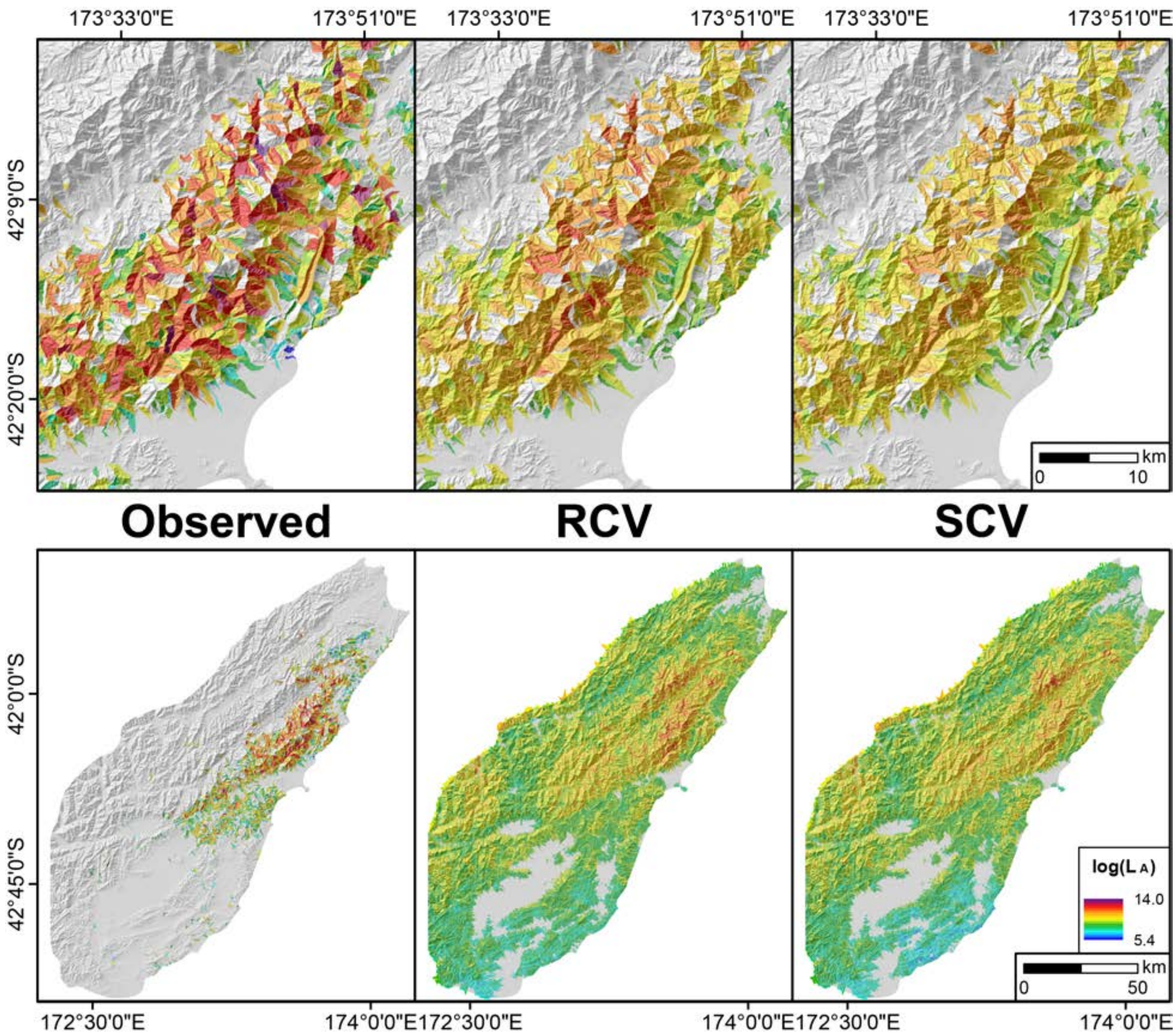

Figure 9: The first row of this figure highlights the details of the main area affected by landslides for which we have observations. The second row shows the whole study area without focusing on the SU for which we measured the landslide area. The first column plots the actual measurements and represents the target variable of our model. The second and third columns report the estimated landslide areas via the RCV and SCV routines.

others call for further improvements. These two elements will be separately discussed in the sections below.

5.1 Supporting arguments

Landslide area correction with respect to slope steepness is something that is hardly considered in most geoscientific contributions, with the exception of very few cases (e.g., Steger et al., 2021). In the context of a model that aimed at predicting landslide size, we consider this a particularly important element to be added to the analytical protocol proposed by Lombardo et al. (2021). Another improvement we introduce is the use of a much richer spatial cross-validation scheme. In their work, Lombardo et al. (2021) originally constrained the spatial cross validation to be generated once. Conversely, the fact that here we focused on a specific site, made it easier for us to replicate the spatial sampling, thus fully randomizing the spatial cross-validation results, in line with what Brenning (2012) prescribed, albeit in a binary context.

The performances we retrieved are satisfying and worth of consideration to extend the landslide area prediction context even further. Figures 7 and 8 provide an exhaustive summary of the extent to which our model is able to estimate the observed landslide areas. This is further translated over the geographic space in Figure 9, where the spatial patterns appear to be matching, albeit the predictive routines still show some progressive deviation from the original A_L values as the cross-validation routines we tested moved from the purely random context to the spatially-constrained one. And yet, with respect to what is available in the literature today, this model offers an important element of discussion that is usually entirely neglected. The binary case pertaining to the susceptibility in fact lacks the information on the level of threat one should expect once a landslide is triggered at a given location. Our model fills this gap and adds a fundamental gusset to strengthen the structure of the available landslide models as of today. We consider our landslide area model a new venue of scientific interest, and we prompt the geoscientific community to explore this framework even further. We already see elements of improvements that can consolidate the concept and role of landslide area prediction within protocols of disaster risk reduction. For instance, the next phase we envision is to combine the areal model together with the traditional susceptibility ones. As things are, the traditional susceptibility framework does not formally account for the expected size of landslides once they are likely triggered in a given slope. However, even our landslide area framework is blind to whether a slope may be prone or not to fail. In turn, this means that these two tools are currently separated, and the next effort should be directed towards merging them into a single product that integrates two important hazard features, namely spatial landslide probability and landslide size. For instance, one could model them separately and then take the product of the two. In such a way, slopes that may morphologically be associated with large failures but are seen to be stable (low probability of occurrence) by the susceptibility component will result in small hazard-proxy value. The same may happen in the case of slopes that are expected to be unstable (high probability of occurrence) but associated with very small landslides. In this scenario, the estimated hazard proxy will also be low. On the contrary, only in situations where high susceptibility is associated with large expected landslides one would obtain a level of such a hazard proxy that would inevitably require attention. Such a scheme will give rise to a completely new landslide hazard framework, providing a full spectrum of probabilistic estimates aimed at aiding the decision-making process for landslide risk reduction.

5.2 Opposing arguments

To provide a critical review of our landslide area model, one should initially take a step back and look at the fundamentals of our model. The fact that it relies on a logarithmic transformation of the landslide area distribution per SU requires some consideration. From a purely mathematical perspective, this framework is sufficient to produce valuable predictive maps as the logarithm is a monotonic transformation. Thus, landslide areas that were smaller in size compared to other SUs in the observed data, will still be relatively smaller in the prediction, irrespective of whether we model directly estimates the landslide extent in m^2 or in $\log(m^2)$. However, two negative elements affect this framework. The most obvious one is that from an interpretation standpoint, one lacks the intuition of what a predicted value would indicate at the $\log(m^2)$ scale. If this argument could still be considered acceptable because of the monotonic transformation mentioned above, reflecting on what this entails in terms of errors does call for potential improvements. A Gaussian likelihood implies by definition that the model focuses on the bulk of the landslide area distribution. In other words, the mean landslide area will be suitably estimated, leaving the tails potentially misrepresented. The left tail, the side of the distribution with very small landslides is definitely of lesser interest. However, a misrepresentation of the right tail, the side of the distribution that hosts very large landslides, can lead to erroneous decisions specifically for the extreme cases, which are also the most dangerous ones. Notably, the performance we produced does not raise concerns to the point of considering our landslide area model inappropriate. However, we envision the next phase of the model development to explore more suitable likelihoods. The log-Gaussian context is particularly appealing because of its easy implementation, and as long as the performance may stay along the lines of what we presented here, the choice of such likelihood can definitely be justified. However, in the hope of further extending the landslide area prediction in different geographic contexts, across different landslide types and triggers, we cannot exclude that the likelihood we chose so far may prove to be insufficient or lead to undesired errors away from the bulk of the distribution. In such cases, extreme-value theory in statistics provides the precise modeling framework to address this issue and we already envision this direction to be the next research and development phase.

6 Conclusions

The data-driven modelling context for landslides has relied essentially on the same toolbox for over five decades now. We believe it is time to review whether some new tools can be added to improve the omnipresent static susceptibility framework and complement the information it provides with other equally important elements. One of these elements certainly consists of how large landslides may be once they initiate, evolve and potentially coalesce into large volumes of materials moving downhill. This information has been traditionally associated with physically-based models, together with other kinematic parameters such as velocity. On the one hand, the landslide kinematics cannot be modeled in detail via data-driven approaches because of the lack of observations. On the other hand though, the landslide area information is contained in any standard landslide polygonal inventory. As a result, one can train data-driven models to learn what environmental characteristics promote small to large landslides and spatially translate this information into maps of expected landslide size. This idea is essentially an uncharted territory within the geoscientific community, with only a few articles currently addressing this issue. However, we see an enormous potential behind it. In fact, physically-based models are constrained to the availability of geotechnical parameters and thus are not well suited to produce estimates over large regions. Our landslide area model circumvents this limitation in the very same way as traditional susceptibility models do. Proxies are used instead of geotechnical parameters to explain the landslide area distribution and allow for statistical inference to be made. Such context opens up a number of potential routes to be taken in the near future, from exploring more technical solutions, to addressing landslide types and triggers of different nature and to test landslide-area-model transferability from a landscape to another. As a result, an entire new toolbox could be made available to scientists and professionals working in disaster risk reduction, supporting the decision making process with a richer hazard information. To promote this type of analyses, we share data and codes in a github repository, accessible at this link.

Acknowledgement

This article was partially supported by King Abdullah University of Science and Technology (KAUST) in Thuwal, Saudi Arabia, Grant URF/1/4338-01-01.

References

Aguilera, Q., Lombardo, L., Tanyas, H. and Lipani, A. (2022) On The Prediction of Landslide Occurrences and Sizes via Hierarchical Neural Networks. Stochastic Environmental Research and Risk Assessment pp. 1–18.

Alvioli, M. and Baum, R. L. (2016) Parallelization of the TRIGRS model for rainfall-induced landslides using the message passing interface. Environmental Modelling & Software **81**(C), 122–135.

Alvioli, M., Marchesini, I., Reichenbach, P., Rossi, M., Ardizzone, F., Fiorucci, F. and Guzzetti, F. (2016) Automatic delineation of geomorphological slope units with r.slopeunits v1.0 and their optimization for landslide susceptibility modeling. Geoscientific Model Development **9**(11), 3975–3991.

Atkinson, P. M. and Massari, R. (1998) Generalised linear modelling of susceptibility to landsliding in the central Apennines, Italy. Computers & Geosciences **24**(4), 373–385.

Ayalew, L., Yamagishi, H., Marui, H. and Kanno, T. (2005) Landslides in Sado Island of Japan: Part II. GIS-based susceptibility mapping with comparisons of results from two methods and verifications. Engineering geology **81**(4), 432–445.

Bordoni, M., Galanti, Y., Bartelletti, C., Persichillo, M. G., Barsanti, M., Giannecchini, R., Avanzi, G. D., Cevasco, A., Brandolini, P., Galve, J. P. et al. (2020) The influence of the inventory on the determination of the rainfall-induced shallow landslides susceptibility using generalized additive models. Catena **193**, 104630.

Brabb, E., Pampeyan, H. and Bonilla, M. (1972) MG 1972. landslide susceptibility in San Mateo County, California. US Geological Survey Miscellaneous Field Studies Map MF-360, scale **1**(62,500).

Brenning, A. (2005) Spatial prediction models for landslide hazards: review, comparison and evaluation. Natural Hazards and Earth System Science **5**(6), 853–862.

Brenning, A. (2012) Spatial cross-validation and bootstrap for the assessment of prediction rules in remote sensing: The R package sperrorest. In 2012 IEEE international geoscience and remote sensing symposium, pp. 5372–5375.

Brenning, A., Schwinn, M., Ruiz-Páez, A. and Muenchow, J. (2015) Landslide susceptibility near highways is increased by 1 order of magnitude in the Andes of southern Ecuador, Loja province. Natural Hazards and Earth System Sciences **15**(1), 45–57.

Bryce, E., Lombardo, L., van Westen, C., Tanyas, H. and Castro-Camilo, D. (2022) Unified landslide hazard assessment using hurdle models: a case study in the Island of Dominica. Accepted in Stochastic Environmental Research and Risk Assessment .

Carrara, A. (1988) Drainage and divide networks derived from high-fidelity digital terrain models. In *Quantitative analysis of mineral and energy resources*, pp. 581–597. Springer.

Castro Camilo, D., Lombardo, L., Mai, P., Dou, J. and Huser, R. (2017) Handling high predictor dimensionality in slope-unit-based landslide susceptibility models through LASSO-penalized Generalized Linear Model. *Environmental Modelling and Software* **97**, 145–156.

Cesca, S., Zhang, Y., Mouslopoulou, V., Wang, R., Saul, J., Savage, M., Heimann, S., Kufner, S.-K., Oncken, O. and Dahm, T. (2017) Complex rupture process of the mw 7.8, 2016, kaikōura earthquake, new zealand, and its aftershock sequence. *Earth and Planetary Science Letters* **478**, 110–120.

Chai, T. and Draxler, R. R. (2014) Root mean square error (RMSE) or mean absolute error (MAE)?–arguments against avoiding RMSE in the literature. *Geoscientific model development* **7**(3), 1247–1250.

Corder, G. W. and Foreman, D. I. (2011) Nonparametric statistics for non-statisticians.

Diederichs, A., Nissen, E., Lajoie, L., Langridge, R., Malireddi, S., Clark, K., Hamling, I. and Tagliasacchi, A. (2019) Unusual kinematics of the Papatea fault (2016 Kaikōura earthquake) suggest anelastic rupture. *Science advances* **5**(10), eaax5703.

Fan, X., Juang, C. H., Wasowski, J., Huang, R., Xu, Q., Scaringi, G., van Westen, C. J. and Havenith, H.-B. (2018) What we have learned from the 2008 Wenchuan Earthquake and its aftermath: A decade of research and challenges. *Engineering Geology* **241**, 25–32.

Fell, R., Corominas, J., Bonnard, C., Cascini, L., Leroi, E., Savage, W. Z. *et al.* (2008) Guidelines for landslide susceptibility, hazard and risk zoning for land-use planning. *Engineering Geology* **102**(3-4), 99–111.

Frattini, P., Crosta, G. and Carrara, A. (2010) Techniques for evaluating the performance of landslide susceptibility models. *Engineering Geology* **111**(1), 62–72.

Godt, J., Sener, B., Verdin, K., Wald, D., Earle, P., Harp, E. and Jibson, R. (2008) Rapid assessment of earthquake-induced landsliding. In *Proceedings of the First World Landslide Forum*, volume 4, pp. 219–222.

Goetz, J. N., Guthrie, R. H. and Brenning, A. (2011) Integrating physical and empirical landslide susceptibility models using generalized additive models. *Geomorphology* **129**(3-4), 376–386.

Guzzetti, F., Carrara, A., Cardinali, M. and Reichenbach, P. (1999) Landslide hazard evaluation: A review of current techniques and their application in a multi-scale study, central italy. *Geomorphology* **31**(1), 181–216.

Hamling, I. J., Hreinsdóttir, S., Clark, K., Elliott, J., Liang, C., Fielding, E., Litchfield, N., Villamor, P., Wallace, L., Wright, T. J. et al. (2017) Complex multifault rupture during the 2016 M w 7.8 Kaikōura earthquake, New Zealand. Science **356**(6334), eaam7194.

Hauenstein, S., Wood, S. N. and Dormann, C. F. (2018) Computing AIC for black-box models using generalized degrees of freedom: A comparison with cross-validation. Communications in Statistics-Simulation and Computation **47**(5), 1382–1396.

Heerdegen, R. G. and Beran, M. A. (1982) Quantifying source areas through land surface curvature and shape. Journal of Hydrology **57**(3-4), 359–373.

Hewitt, A. E. et al. (2010) New zealand soil classification. Landcare research science series (1).

Huang, F., Tao, S., Chang, Z., Huang, J., Fan, X., Jiang, S.-H. and Li, W. (2021) Efficient and automatic extraction of slope units based on multi-scale segmentation method for landslide assessments. Landslides pp. 1–17.

Intrieri, E., Gigli, G., Mugnai, F., Fanti, R. and Casagli, N. (2012) Design and implementation of a landslide early warning system. Engineering Geology **147**, 124–136.

Jasiewicz, J. and Stepinski, T. F. (2013) Geomorphons—a pattern recognition approach to classification and mapping of landforms. Geomorphology **182**, 147–156.

Jiao, Y.-Y., Zhang, H.-Q., Tang, H.-M., Zhang, X.-L., Adoko, A. C. and Tian, H.-N. (2014) Simulating the process of reservoir-impoundment-induced landslide using the extended DDA method. Engineering Geology **182**, 37–48.

Kaiser, A., Balfour, N., Fry, B., Holden, C., Litchfield, N., Gerstenberger, M., D'anastasio, E., Horspool, N., McVerry, G., Ristau, J. et al. (2017) The 2016 kaikōura, new zealand, earthquake: preliminary seismological report. Seismological Research Letters **88**(3), 727–739.

Kenney, J. F. and Keeping, E. (1962) Linear regression and correlation. Mathematics of statistics **1**, 252–285.

Kirschbaum, D. and Stanley, T. (2018) Satellite-Based Assessment of Rainfall-Triggered Landslide Hazard for Situational Awareness. Earth's Future **6**(3), 505–523.

Lee, S.-J., Chen, H.-W., Liu, Q., Komatitsch, D., Huang, B.-S. and Tromp, J. (2008) Three-dimensional simulations of seismic-wave propagation in the Taipei basin with realistic topography based upon the Spectral Element Method. Bulletin of the Seismological Society of America **98**, 253–264.

Lepore, C., Kamal, S. A., Shanahan, P. and Bras, R. L. (2012) Rainfall-induced landslide susceptibility zonation of puerto rico. Environmental Earth Sciences **66**(6), 1667–1681.

Lilburne, L., Hewitt, A. and Webb, T. (2012) Soil and informatics science combine to develop S-map: A new generation soil information system for New Zealand. Geoderma **170**, 232–238.

Lin, Q., Lima, P., Steger, S., Glade, T., Jiang, T., Zhang, J., Liu, T. and Wang, Y. (2021) National-scale data-driven rainfall induced landslide susceptibility mapping for China by accounting for incomplete landslide data. Geoscience Frontiers **12**(6), 101248.

Loche, M., Lombardo, L., Gorum, T., Tanyas, H. and Scaringi, G. (2022) Distinct susceptibility patterns of active and relict landslides reveal distinct triggers: A case in northwestern Turkey. Remote Sensing **14**(6), 1321.

Lombardo, L., Bakka, H., Tanyas, H., van Westen, C., Mai, P. M. and Huser, R. (2019) Geostatistical modeling to capture seismic-shaking patterns from earthquake-induced landslides. Journal of Geophysical Research: Earth Surface **124**(7), 1958–1980.

Lombardo, L. and Mai, P. M. (2018) Presenting logistic regression-based landslide susceptibility results. Engineering geology **244**, 14–24.

Lombardo, L., Opitz, T., Ardizzone, F., Guzzetti, F. and Huser, R. (2020) Space-time landslide predictive modelling. Earth-Science Reviews p. 103318.

Lombardo, L. and Tanyas, H. (2020) Chrono-validation of near-real-time landslide susceptibility models via plug-in statistical simulations. Engineering geology **278**, 105818.

Lombardo, L. and Tanyas, H. (2021) From scenario-based seismic hazard to scenario-based landslide hazard: fast-forwarding to the future via statistical simulations. Stochastic Environmental Research and Risk Assessment pp. 1–14.

Lombardo, L., Tanyas, H., Huser, R., Guzzetti, F. and Castro-Camilo, D. (2021) Landslide size matters: A new data-driven, spatial prototype. Engineering Geology **293**, 106288.

Luo, L., Lombardo, L., van Westen, C., Pei, X. and Huang, R. (2021) From scenario-based seismic hazard to scenario-based landslide hazard: rewinding to the past via statistical simulations. Stochastic environmental research and risk assessment pp. 1–22.

Massey, C., Townsend, D., Lukovic, B., Morgenstern, R., Jones, K., Rosser, B. and de Vilder, S. (2020) Landslides triggered by the mw7. 8 14 november 2016 kaikōura earthquake: an update. Landslides **17**(10), 2401–2408.

Massey, C., Townsend, D., Rathje, E., Allstadt, K. E., Lukovic, B., Kaneko, Y., Bradley, B., Wartman, J., Jibson, R. W., Petley, D. et al. (2018) Landslides triggered by the 14 november 2016 mw 7.8 kaikōura earthquake, new zealandlandslides triggered by the 14 november 2016 mw 7.8 kaikōura earthquake, new zealand. Bulletin of the Seismological Society of America **108**(3B), 1630–1648.

Mayer, D. and Butler, D. (1993) Statistical validation. Ecological modelling **68**(1-2), 21–32.

Melosh, H. (1986) The physics of very large landslides. Acta Mechanica **64**(1), 89–99.

Mm, M. (2012) Statistics corner: A guide to appropriate use of Correlation coefficient in medical research. Malawi Med J **24**(3), 69–71.

Molnar, C. (2020) Interpretable machine learning. Lulu. com.

Nandi, A. and Shakoor, A. (2010) A GIS-based landslide susceptibility evaluation using bivariate and multivariate statistical analyses. Engineering Geology **110**(1-2), 11–20.

Nowicki, M. A., Wald, D. J., Hamburger, M. W., Hearne, M. and Thompson, E. M. (2014) Development of a globally applicable model for near real-time prediction of seismically induced landslides. Engineering Geology **173**, 54–65.

Nowicki Jessee, M., Hamburger, M., Allstadt, K., Wald, D., Robeson, S., Tanyas, H., Hearne, M. and Thompson, E. (2018) A Global Empirical Model for Near-Real-Time Assessment of Seismically Induced Landslides. Journal of Geophysical Research: Earth Surface **123**(8), 1835–1859.

Ohlmacher, G. C. (2007) Plan curvature and landslide probability in regions dominated by earth flows and earth slides. Engineering Geology **91**(2), 117–134.

Petschko, H., Brenning, A., Bell, R., Goetz, J. and Glade, T. (2014) Assessing the quality of landslide susceptibility maps—case study Lower Austria. Natural Hazards and Earth System Sciences **14**(1), 95–118.

Reichenbach, P., Rossi, M., Malamud, B. D., Mihir, M. and Guzzetti, F. (2018) A review of statistically-based landslide susceptibility models. Earth-Science Reviews **180**, 60–91.

Schober, P., Boer, C. and Schwarte, L. A. (2018) Correlation coefficients: appropriate use and interpretation. Anesthesia & Analgesia **126**(5), 1763–1768.

Schratz, P., Muenchow, J., Iturritxa, E., Richter, J. and Brenning, A. (2019) Hyperparameter tuning and performance assessment of statistical and machine-learning algorithms using spatial data. Ecological Modelling **406**, 109–120.

Steger, S., Brenning, A., Bell, R. and Glade, T. (2016) The propagation of inventory-based positional errors into statistical landslide susceptibility models. Natural Hazards and Earth System Sciences **16**(12), 2729–2745.

Steger, S., Brenning, A., Bell, R. and Glade, T. (2017) The influence of systematically incomplete shallow landslide inventories on statistical susceptibility models and suggestions for improvements. Landslides **14**(5), 1767–1781.

Steger, S., Mair, V., Kofler, C., Pittore, M., Zebisch, M. and Schneiderbauer, S. (2021) Correlation does not imply geomorphic causation in data-driven landslide susceptibility modelling–Benefits of exploring landslide data collection effects. Science of the total environment **776**, 145935.

Tanyaş, H., van Westen, C., Allstadt, K., Nowicki, A. J. M., Görüm, T., Jibson, R., Godt, J., Sato, H., Schmitt, R., Marc, O. and Hovius, N. (2017) Presentation and Analysis of a Worldwide Database of Earthquake-Induced Landslide Inventories. Journal of Geophysical Research: Earth Surface **122**(10), 1991–2015.

Tanyaş, H., Görüm, T., Kirschbaum, D. and Lombardo, L. (2022) Could road constructions be more hazardous than an earthquake in terms of mass movement? Natural Hazards pp. 1–25.

Tanyas, H., Gorum, T. and Lombardo, L. (2022) An open dataset for landslides triggered by the 2016 Mw 7.8 Kaikōura earthquake, New Zealand. Landslides .

Tanyaş, H., Hill, K., Mahoney, L., Fadel, I. and Lombardo, L. (2022) The world's second-largest, recorded landslide event: Lessons learnt from the landslides triggered during and after the 2018 mw 7.5 papua new guinea earthquake. Engineering Geology **297**, 106504.

Tanyas, H. and Lombardo, L. (2019) Variation in landslide-affected area under the control of ground motion and topography. Engineering geology **260**, 105229.

Titti, G., van Westen, C., Borgatti, L., Pasuto, A. and Lombardo, L. (2021) When enough is really enough? on the minimum number of landslides to build reliable susceptibility models. Geosciences **11**(11), 469.

Ulrich, T., Gabriel, A.-A., Ampuero, J.-P. and Xu, W. (2019) Dynamic viability of the 2016 Mw 7.8 Kaikōura earthquake cascade on weak crustal faults. Nature communications **10**(1), 1–16.

Van Westen, C., Rengers, N. and Soeters, R. (2003) Use of geomorphological information in indirect landslide susceptibility assessment. Natural hazards **30**(3), 399–419.

Van Westen, C. J., Castellanos, E. and Kuriakose, S. L. (2008) Spatial data for landslide susceptibility, hazard, and vulnerability assessment: An overview. Engineering geology **102**(3-4), 112–131.

Van Westen, C. J., Rengers, N., Terlien, M. and Soeters, R. (1997) Prediction of the occurrence of slope instability phenomenal through GIS-based hazard zonation. Geologische Rundschau **86**(2), 404–414.

Vorpahl, P., Elsenbeer, H., Märker, M. and Schröder, B. (2012) How can statistical models help to determine driving factors of landslides? Ecological Modelling **239**, 27–39.

Wang, H., Zhang, L., Luo, H., He, J. and Cheung, R. (2021) AI-powered landslide susceptibility assessment in Hong Kong. Engineering Geology **288**, 106103.

Webb, T. H. and Lilburne, L. (2011) Criteria for defining the soil family and soil sibling: The fourth and fi Manaaki Whenua Press, Landcare Research.

Willmott, C. J. and Matsuura, K. (2005) Advantages of the mean absolute error (MAE) over the root mean square error (RMSE) in assessing average model performance. Climate research **30**(1), 79–82.

Wood, S. N. and Augustin, N. H. (2002) GAMs with integrated model selection using penalized regression splines and applications to environmental modelling. Ecological modelling **157**(2-3), 157–177.

Worden, C. and Wald, D. (2016) ShakeMap manual online: Technical manual, user's guide, and software guide. US Geol. Surv. .

Yamada, M., Mangeney, A., Matsushi, Y. and Matsuzawa, T. (2018) Estimation of dynamic friction and movement history of large landslides. Landslides **15**(10), 1963–1974.

Yeon, Y.-K., Han, J.-G. and Ryu, K. H. (2010) Landslide susceptibility mapping in Injae, Korea, using a decision tree. Engineering Geology **116**(3-4), 274–283.

Zevenbergen, L. W. and Thorne, C. R. (1987) Quantitative analysis of land surface topography. Earth surface processes and landforms **12**(1), 47–56.

Zuur, A. F., Ieno, E. N. and Elphick, C. S. (2010) A protocol for data exploration to avoid common statistical problems. Methods in ecology and evolution **1**(1), 3–14.

Zuur, A. F., Ieno, E. N., Walker, N. J., Saveliev, A. A. and Smith, G. M. (2009) GLM and GAM for absence–presence and proportional data. In Mixed effects models and extensions in ecology with R, pp. 245–259. Springer.